Wear Comfort of Heat Storage/Release Fabrics Containing Al$_2$O$_3$/Graphite Yarns

Hyun Ah Kim*

Korea Research Institute for Fashion Industry, Daegu 41028, Korea
(Received November 14, 2020; Revised May 24, 2021; Accepted June 9, 2021)

Abstract: This study examined the wear comfort properties of Al$_2$O$_3$/graphite-imbedded fabrics with sheath/core and dispersed PET yarns. The moisture absorption and drying characteristics were measured by a moisture management tester (MMT) method, and thermal property by a KES-F7 system. The results were discussed in terms of the ceramic-imbedded yarn structure, which was verified by the far-infrared emissivity and the maximum surface temperature measured by a light heat emission apparatus. In addition, the tactile hand feel of the fabric specimens was estimated from the fabric mechanical properties by a fabric assurance simple testing (FAST) system. The water absorption and drying properties of the Al$_2$O$_3$/graphite sheath/core yarn fabric were inferior to those of the dispersed yarn fabric, and the heat retention rate was lower than that of the dispersed yarn fabric with lower thermal conductivity and higher Q$_{max}$ value. These results revealed that the Al$_2$O$_3$/graphite sheath/core yarn fabric has inferior wear comfort properties compared to those of the dispersed yarn fabric, which was attributed to the lower heat release from the core part of the sheath/core yarn than that from the dispersed yarn with Al$_2$O$_3$/graphite particles distributed over the whole yarn cross-section. This was further verified by the lower emissivity and maximum surface temperature of the sheath/core yarn fabric than those of the dispersed yarn fabric. However, the sheath/core yarn fabric exhibited slightly a softer tactile hand feel compared to the dispersed yarn fabric. Both sheath/core and dispersed yarn fabrics exhibited better wear comfort properties than the regular PET fabric did, but showed an uncomfortable tactile hand feel compared to the regular PET fabric.

Keywords: Wear comfort, Heat storage and release, MMT, KES-F7, FAST

Introduction

Most recently, the interactions between the heat storage characteristics of the fabrics made from inorganic ceramic-imbedded yarns and the far-infrared radiation emitted from its yarns have attracted considerable attention. According to previous study [1], infrared zone is divided into three types of region, near-IR (NIR, 0.8-2.5 μm), mid-IR (MIR, 2.5-16.7 μm) and in particular, 7.5 and 14 μm region is sometimes referred to as the far-infrared (FIR) in the textile field. Anderson *et al*. [2] reported that far-infrared properties are of particular importance when considering interactions with the human body, as, at nominal skin temperature, much of the body's emissive radiative power is centered in the far-infrared between 7 and 14 μm. Investigating various studies [1-5] carried out up to now, inorganic particles such as ZrC, Al$_2$O$_3$, SiO$_2$, TiO$_2$ and graphite imparted the heat storage and release properties of the yarns and fabrics with high emissivity and emissive energy at the wavelength zone of the far-infrared. Furthermore, the findings of these studies were focused on the far-infrared emissivity and temperature rise due to high far-infrared emissivity. Inorganic ceramic-imbedded yarn manufacturing technology is a positive method for achieving the heat storage/release properties of the textile material by far-infrared radiation. Many Japanese companies have commercialized ceramic-imbedded heat storage yarns using mostly ZrC inorganic particles. Although

these commercialized heat storage/release yarns provide some technical information, the wear comfort properties, including the heat storage/release properties of the ceramic-imbedded woven fabrics, are less known due to complicated experimental reasons. On the other hand, many studies [4-6] related to the heat storage/release of the fabrics have been carried out using different types of ceramic-imbedded yarn. In early years, Furuta *et al*. [4] studied the moisture permeability of a heat storage fabric made of ZrC-imbedded PET filament. They reported the increase of the moisture permeability of the ZrC-imbedded fabric due to heat released from the ZrC-imbedded PET filament. Similarly, Bahng *et al*. [5] developed the heat-release PET filament by imbedding ceramic powder and reported the rapid perspiration absorption and fast drying properties of the ceramic-imbedded PET fabric. Kuo *et al*. [6] reported the effect of the far-infrared emission in the polypropylene filament imbedded with nano-SiO$_2$ and nano-ZnO, and reported that the temperature increment induced by the far-infrared emission was 8.6 °C, which was 1.43 times higher than that of the pure PP, 1.53 times higher than that of PET and 1.75 times higher than that of nylon. On the other hand, recently, the wear comfort of the heat storage fabric was examined via thermal manikin experiment in relation to the emissivity of far-infrared emitted from the ceramic-imbedded yarns. Kim *et al*. [7,8] examined the far-infrared emission characteristics of the ZrC-imbedded knitted fabric and reported the wear comfort of the ZrC-imbedded woven fabric via thermal manikin experiment. Most of the previous investigations on

*Corresponding author: ktufl@krifi.re.kr

the ceramic-imbedded commercialized textiles were carried out using ZrC ceramic powder, and these studies concluded that ZrC absorbs the heat emitted from the human body or reflects the far-infrared radiation, which prevents the heat in the clothing and human body from flowing out. Therefore, the heat storage of the ZrC-imbedded fabric is achieved by transforming to the thermal energy after absorbing near infrared light from sunlight. On the other hand, earlier studies [9-12] used different ceramic materials, such as charcoal, ZnO, Al_2O_3, SiO_2 and TiO_2, on polypropylene and other filaments to enhance the far-infrared emission related to the heat storage and release properties. Lin *et al*. [9] examined the relationship between the far-infrared ray emission property and the absorption performance of bamboo/charcoal-imbedded polyvinyl alcohol (PVA) fibers. They reported that the mean emission rate of the far-infrared radiation between 8-14 μm wavelength from the bamboo/charcoal-imbedded PVA fibers increased with increasing bamboo/charcoal content. Lin *et al*. [10] studied the effects of ceramic powders such as Al_2O_3, TiO_2 and SiO_2 mixed with polypropylene homo-copolymer on the far-infrared emissivity emanating from plastic composites. In their study on the heat storage and release by the far-infrared ray emission from the carbonized powder in the yarn, Lin and Chang [11] examined the heat retention by the far-infrared ray emission emanating from the carbonized powder of the charcoal fibers in the nonwoven fabrics. In addition, Lin *et al*. [12] reported the far-infrared emissivity and air permeability of knitted fabric made of stainless steel/polyester/bamboo charcoal wrapped yarns. According to the previous studies carried out by Lin *et al*. [9,11,12], carbonized powder and charcoal imbedded with inorganic particles in the yarns imparted heat release and storage properties of the yarns. Graphite, archaically referred to as plumbago, is a crystalline form of the element carbon with its atoms arranged in a hexagonal structure, which is analogous to charcoal and carbon [13]. Graphite is a good conductor of heat and electrically. Its high thermal conductivity makes it useful in solar panels. The spectral emissivity of dull surfaced graphite is 0.9 and approaching 0.99 near sublimation temperatures of 3600K [13]. Recently, observing the superior thermal characteristics of the graphite, an attempt for research was performed in textiles using the graphite nano-particles. Kim and Kim [14] examined heat storage and release properties of Al_2O_3/graphite and ZrC/graphite imbedded yarns and their fabrics. They [14] reported that heat release characteristics of the ZrC/graphite imbedded fabrics were superior to those of the ZrC imbedded fabric, which was carried out by them [7,8], i.e. the surface temperature of the ZrC/graphite imbedded fabric by a light heat-emission apparatus was higher than that of the ZrC imbedded fabric, which indicates positive effect of graphite imbedded in the yarns in the heat release and

storage properties of the fabric. On the other hand, the various wear comfort properties of the fabrics using a thermal manikin and wearer trials with human subjects was recently carried out by investigating the heat storage/release properties of the PET fabrics imbedded with inorganic nano-powders such as ZrC, Al_2O_3 and graphite [14]. They reported that the wear comfort and heat storage/release properties of the ZrC/graphite dispersed PET fabric appeared to be superior to those of the Al_2O_3/graphite dispersed fabric. Moreover, the ZrC/graphite dispersed fabric made of yarns dispersed over the whole yarn cross-section exhibited a superior tactile hand feel to the Al_2O_3/graphite dispersed fabric. However, ZrC/graphite dispersed fabric showed some issue point in color after dyeing process due to black color of ZrC nano-particles, i.e. the ZrC/graphite imbedded yarns dispersed over the whole yarn cross-section gave the fabric a grey color, which was not a fashionable and vivid color. These results indicated why most of the ceramic imbedded fabrics commercialized in various companies (Unitika, Kuraray, Mitsubishi-rayon etc.) were focused on ZrC-imbedded fabrics (not include graphite), still more, ZrC nano-powders were imbedded in the core, not dispersed over the whole yarn cross-section. Summarizing previous study, even if ZrC/graphite dispersed fabric has a superior heat storage/release properties compared to ZrC/graphite sheath/core fabric, it could not commercialize because of color problem, whereas, Al_2O_3/graphite dispersed fabric exhibited bright and superior colors than ZrC/graphite dispersed fabric. The results of the previous study suggested that the comparison of the heat storage/release characteristics including tactile hand between Al_2O_3/graphite dispersed and sheath/core fabrics is needed more to improve both thermal property and fabric hand without color problem in dyeing process. Therefore, to follow up our previous research, this study examined the differences of heat storage/release properties and wear comfort between Al_2O_3/graphite dispersed and sheath/core fabrics. For this purpose, the Al_2O_3/graphite-imbedded sheath/core and dispersed PET filaments were spun on a conjugated melt spinning machine and three types of fabric specimen were woven using these two types of yarn and regular PET yarn, respectively. The wear comfort properties such as the water absorption and drying properties, and heat retention rate (I) were measured and compared with those of the regular PET fabric using a moisture management tester (MMT) and a KES-F7 thermal property measuring apparatus, respectively. In addition, these results were verified by the far-infrared emissivity and the maximum surface temperature related to the heat storage/release properties of the Al_2O_3/graphite dispersed and sheath/core fabrics. Finally, the tactile hand feel of the Al_2O_3/graphite dispersed and sheath/core fabrics was estimated from the fabric mechanical properties and the results are discussed in comparison with those of the regular PET fabric.

Experimental

Spinning of Partially Oriented Yarn (POY) Specimens

The Al_2O_3/graphite-imbedded sheath/core PET POY (120d/24f) was spun using a pilot conjugated melt spinning machine (TW-536, TMT Co. Ltd., Japan). The bi-component conjugated PET POY yarn composed of sheath/core (composition: 50 wt.% each) was spun, and the dispersed yarn was spun with a changed pack and the spinning nozzle on the same melt spinning machine. The sheath/core yarn was spun using two types of master batch chip with a concentration of 10 wt.% Al_2O_3 and 5 wt.% graphite mixed with PET polymer. The master batch chips composed of either Al_2O_3 (10 wt.%) and PET polymer (90 wt.%) or graphite (5 wt.%) and PET polymer (95 wt.%) were first made using a compounding equipment (SM platek Co. Ltd., Korea), and then the Al_2O_3 master batch chips (3.5 kg) and graphite ones (1.0 kg) were mixed together with 20.5 kg of PET polymer and extruded into the core part of the spinneret hole, and the PET polymer (25 kg) was extruded into the sheath part, which gave a total mixing ratio for the yarn of 0.7 wt.% Al_2O_3 and 0.1 wt.% graphite. The resulting particle sizes of Al_2O_3 and graphite ranged from 0.5 to 0.6 μm, and they were then filtered using a mesh ranging 600 to 800 nm. In the same manner, Al_2O_3/graphite-dispersed PET POY, (120d/24f) was spun using the master batch chip made previously. Spinning was carried out by changing the pack and nozzle in the conjugated spinning machine using the PET polymer (45.5 kg) mixed with each master batch chip (3.5 kg/1.0 kg) of the Al_2O_3 and graphite, and the total mixing ratios (0.7 wt.%, Al_2O_3 and 0.1 wt.%, graphite) were the same as those of the sheath/core yarn specimen. Table 1 lists the specification of the sheath/core, dispersed and regular PET filaments. In Table 1, yarn specimens were made with 24 single filaments on the melt spinning machine.

First, Al_2O_3/graphite sheath/core PET POY yarn was spun using mixed polymer melted with Al_2O_3, graphite and PET chips in the core and PET polymer in the sheath. Yarn linear density of POY was 120d/24f, and then it was drawn into 70d/24f in the texturing machine. Dispersed PET POY was spun using a mixed polymer melted with Al_2O_3, graphite and PET chips. Yarn linear density of POY was 120d/24f and then it was drawn into 70d/24f. As a control yarn, regular PET yarn (75d/72f) was used to prepare fabric specimen 3, which was supplied by Hyosung Co. Ltd. (Korea). Schematic yarn cross-sections imbedded with Al_2O_3, TiO_2 and graphite particles were drawn in Table 1.

The PET polymer was supplied by Hyosung Co. Ltd. (Korea); the intrinsic viscosity was 0.665, the glass transition temperature (Tg) was 80.7 °C, the melting temperature was 252 °C, and the content of TiO_2 was 0.36 %. The spinning system was equipped with a 24-hole spinneret with a capillary diameter of 0.2 mm and a length of 0.5 mm. The spinning temperature in the pack was changed from 280 °C to 290 °C to determine the optimal spinnability condition, and the temperature in the spin tube was determined to be 287 °C. The heating temperature in the extruder ranged from 287 °C to 290 °C in the core and from 310 °C to 315 °C in the sheath. The 1st godet roller speed and temperature were 3,160 m/min and 80 °C, respectively, and the 2nd were 3,100 m/min and 105 °C, respectively. The speed on the take-up winder was 3,100 m/min. The spinning conditions of the dispersed yarns were nearly the same as those of the Al_2O_3/graphite sheath/core yarns except the heating temperature ranged 290 to 295 °C in the extruder. POY 120d/24f was texturized as 75d/24f under the following conditions : draw ratio of 1.76, velocity ratio of 1.36, heater temperature of 180 °C and feed speed of 450 m/min on the belt-type texturing machine (Murata 33H, Japan).

Table 1. Specification of the sheath/core, dispersed and regular PET yarn specimens

Specimens (yarn)	Yarn count (d/f)	Core mixed PET polymer				Sheath PET polymer	Total mixing ratio (wt.%)		Yarn cross section
		PET polymer (kg)	M/B (kg)		Total (kg)	Total (kg)	Al_2O_3	Graphite	
			Al_2O_3 (10 wt.%) +PET(90 wt.%)	Graphite (5 wt.%) +PET(95 wt.%)					
1 Al_2O_3/graphite sheath/core PET	75/24	20.5	3.5	1.0	25	25	0.7	0.1	
2 Al_2O_3/graphite dispersed PET	75/24	45.5	3.5	1.0	50	-	0.7	0.1	
3 Regular PET	75/72	Existing yarn as a control yarn (TiO_2: 0.36 %)							

M/B: master batch.

Table 2. Specification of fabric specimens

Specimens (fabric)	Yarn count (d/f)		Fabric density (ends, picks/cm)		Thickness		Weight		Weave pattern
	Wp	Wf	Wp	Wf	Mean (mm)	CV (%)	Mean (g/m²)	CV (%)	
1 Al$_2$O$_3$/graphite sheath/core PET	70/34 PA	75/24 S/C PET	51.6	35.4	0.128	0.53	84.2	2.4	Plain
2 Al$_2$O$_3$/graphite dispersed PET	70/34 PA	75/24 disp. PET	51.6	35.4	0.134	0.45	85.4	2.6	Plain
3 Regular PET	70/34 PA	75/72 reg. PET	51.6	35.4	0.122	0.41	83.1	2.7	Plain

PA: polyamide, PET: polyethylene terephthalate, S/C: sheath/core, d/f: denier/filament.

Preparation of Fabric Specimens

Three types of woven fabric were made on the water jet loom (ZW 315X, Tsudakoma, Japan) using nylon 70d/34f in the warp with three types of weft yarn: an Al$_2$O$_3$/graphite sheath/core PET yarn, an Al$_2$O$_3$/graphite-dispersed PET yarn, and a regular PET yarn which was prepared with existing commercial yarn as the control yarn. Weave pattern of the fabrics was a plain. The grey fabric specimens were scoured in the CPB scouring machine, washed and dyed in the rapid dyeing machine, and finally washed and dried in the tenter machine. Table 2 lists the specifications of the fabric specimens.

Elemental Analysis of the Yarn Specimens and Far-infrared Emission Measurement

Elemental analysis of the Al$_2$O$_3$/graphite sheath/core, dispersed yarns and regular PET yarn specimens was carried out by using an energy disperse X-ray spectroscopy (EDS, Jeol LV 8500, Japan). The far-infrared emission characteristics of the Al$_2$O$_3$/graphite sheath/core, dispersed and regular PET yarn specimens were measured using a Fourier transform infrared (FT-IR) spectrometer (Midac M 2400-C, USA). The emissivity and emissive power of the yarn specimens were measured at 40 °C in the wavelength range of 5-20 μm. The emissivity and emissive power measured were compared and discussed with thermal radiation measurement in relation to heat storage/release characteristics of the yarn specimens, which was also verified in previous studies carried out by Kim and Kim [7,8,14]. Cross-sections of the yarns and fabrics were measured by SEM (S-4300, Hitachi Co., Japan).

Thermal Radiation Measurement of the Fabric Specimens

Thermal radiation measurement by light emission was carried out using a light heat emission apparatus (UL chemical, Korea), as shown in Figure 1. The lamp set on the upper position of the light heat emission apparatus was a white tungsten one (Iwasaki, 3200K, Japan). Specimens sized 10×10 cm were prepared at a temperature of 20±2 °C and relative humidity (RH) of 65±5 %. The heat emission bulb, separated from the specimen by 30 cm, was switched on and the temperature increase in the specimen was
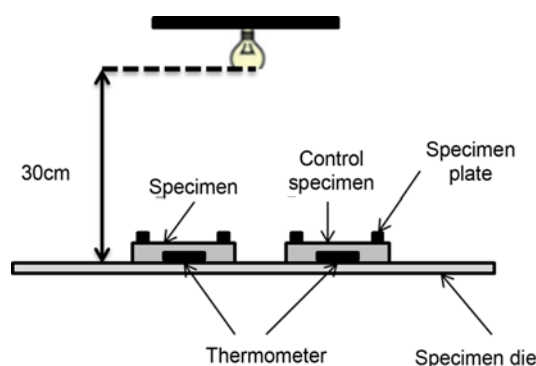

Figure 1. Schematic diagram of a light heat emission apparatus.

measured with a thermometer equipped with contact-type sensor (PT 100, Omega engineering, USA) according to the measuring time.

Measurement of the Heat Retention Rate of the Fabric Specimens

The heat retention rate (I) of the fabric specimens was measured using a KES-F7 system (Kato Tech. Co., Japan) at 20±1 °C and 70±5 % RH, and was calculated using equation (1).

$$I = \left(1 - \frac{b}{a}\right) \times 100 \tag{1}$$

where, a is the heat emanating from the test plate (W), and b the heat emanating from the fabric specimen mounted (W). In addition, the thermal conductivity (K) and maximum heat flow at transient state (Q$_{max}$) were assessed using equations (2) and (3) to investigate the thermal properties of the heat storage fabric specimens. An average of the ten readings for each specimen was reported.

$$K = W \cdot d / A \cdot \Delta T \tag{2}$$

where, K is the thermal conductivity (W/cm °C), W the heat loss (W), d the fabric specimen thickness (cm), A the fabric specimen area (cm²), and ΔT the temperature difference (°C).

$$Q_{\max} = A \int q(t)dt\Big|_{\max} = -MC \int \frac{dT(\tau)}{d\tau} d\tau\Big|_{\max} \qquad (3)$$

where, $q(t)$ is the heat absorption rate per unit area of the specimen (cal/sec·cm^2), M the mass of the heat plate, C the specific heat of heat plate (cal/g·^{o}C), and $dT(\tau)/d\tau$ the heat decrease rate of heat plate.

Measurement of the Moisture Absorption and Drying Properties

The moisture absorption and drying properties of the three fabric specimens were measured using a MMT. The measurement was carried out in an air-conditioned room (temp : 20±1 ^{o}C and R.H. : 65±2 %) according to the standard AATCC (American Association of Textile Chemists and Colorists) Test Method 15 (AATCC, 2002). Five pieces of each of the three fabric specimens were prepared as 80× 80 cm square specimens. The MMT was designed to measure the liquid moisture transport behaviors in multiple directions. The measured electrical resistance is related to the water content in the fabric specimens according to the following four measured items. The wetting time (sec) is measured on the top and bottom surfaces of the fabric specimen and is the time period in which the top and bottom surfaces of the fabric just start to become wetted. The absorption rate (%) is the average moisture absorption ability of the fabric, which is calculated automatically by the initial slope of the water content versus time curve. The maximum wetted radius (MWR, mm) is the radius of the circle, which is automatically recorded in this apparatus. The spreading speed (mm/sec) is defined as the velocity from the center of the wetted ring to the MWR, which is calculated automatically as MWR/t, where t is the time to reach the maximum wetted ring.

Measurement of the Fabric Mechanical Properties

The mechanical properties of the fabric specimens were measured using a fabric assurance simple testing (FAST) system [15]. The compressibility was measured using a FAST-1 measuring apparatus. The surface thickness (ST) was calculated as the difference in the thickness of a fabric at a compression of 2 gf/cm^2 and 100 gf/cm^2. The bending

rigidity (B, μN·m) was calculated using C, as shown in equation (4) [15], which was measured using a FAST-2 measuring device.

$$B = W \times C^3 \times 9.52 \times 10^{-6} \qquad (4)$$

where C is the bending length (mm) and W the weight per unit area of fabric (cN/m^2). The extensibility was measured at a load of 19.42 cN/cm and 98.04 cN/cm (denoted as E20 and E100, respectively) using a FAST-3 system. The shear rigidity (G, N/m) was calculated using EB5, as shown in equation (5) [15], which was measured using a FAST-3 measuring device.

$$G = (123/EB5) \times 1 \text{ N/m} \qquad (5)$$

where EB5 is the bias extension under a 4.85 cN/cm width in percentage.

Results and Discussion

Characteristics of the Ceramic-imbedded PET Yarn Specimens

Figures 2(a), (b) and (c) show SEM images of the yarn specimens. In comparing (a) and (b), no clear boundary line was evident between the sheath and core in the yarn specimen (a), which was nearly the same as the image shown in Figure 2(b). Some Al$_2$O$_3$ particles in the yarn specimen (a) appeared at the sheath part of the yarn cross-sections, even though Al$_2$O$_3$ particles were imbedded in the core part during the spinning process, which was attributed to the dispersal of the Al$_2$O$_3$ particles in the yarn by swelling as the filament was extruded from the orifice of the spinneret. More white spots were accumulated in the cross-section of the sheath/core PET yarn around the center than around other places, as shown in Figure 2(a), whereas the white spots in the dispersed and regular PET yarns were distributed over the whole yarn cross-section, as shown in Figure 2(b) and (c).

This SEM result was verified by the elemental analysis results that are presented in Figures 3(a)-(c) for the Al$_2$O$_3$/ graphite sheath/core, dispersed and regular PET yarns, respectively. Peaks were observed for both Al (Figure 3(a) and 3(b)) imbedded in the sheath/core and dispersed PET
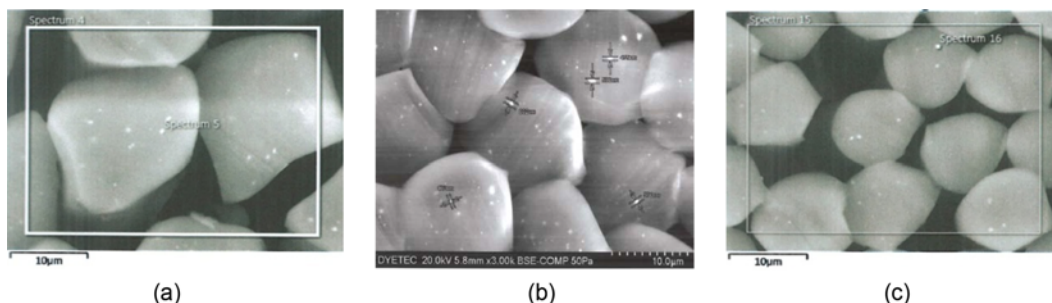

Figure 2. SEM images of the cross-sections of yarn specimens (x1200); (a) yarn specimen 1, (b) yarn specimen 2, and (c) yarn specimen 3.
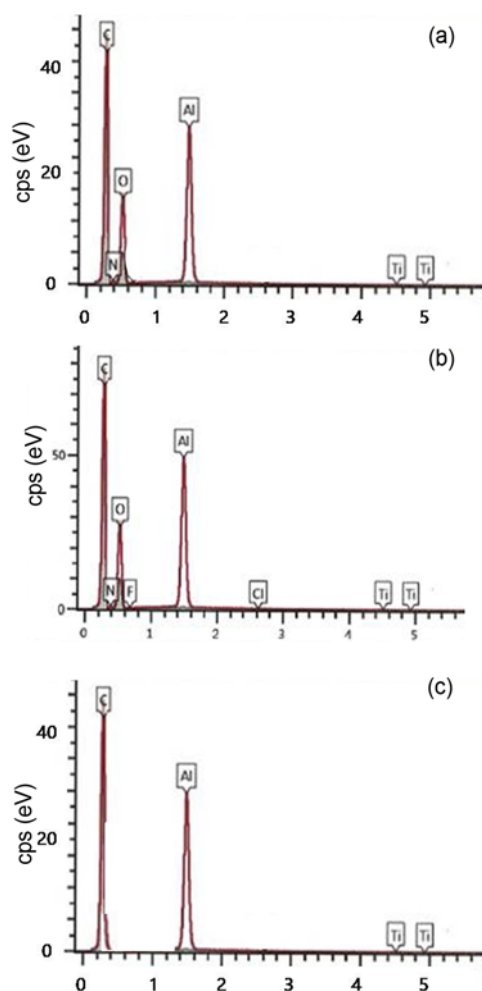
Figure 3. Elemental analysis of the yarn specimens; (a) yarn specimen 3, (b) yarn specimen 2, and (a) yarn specimen 3.

yarns and Ti (Figure 3(c)) imbedded in the regular PET yarns. In particular, Tipeaks were also observed in Figures 3(a) and (b), because the PET polymer used in this study included TiO_2 (0.36 wt.%) as a delustre agent.

Heat Release Characteristics of the Al_2O_3/Graphite Sheath/Core and Dispersed PET Yarn Fabrics

Figure 4 presents the light heat emission diagram of the three fabric specimens, which shows the temperature rise on the fabric surface according to the time lapsed by the heat emanating from the fabric as the light was irradiated from 30 cm above the fabric specimen. As shown in Figure 4, the maximum temperatures by heat emitted in the fabric due to light irradiated for 10 min of the Al_2O_3/graphite sheath/core (specimen 1) and dispersed fabrics (specimen 2) were higher than that of the regular PET fabric (specimen 3). This was attributed to the heat released from the far-infrared emitted from the Al_2O_3 and graphite imbedded in the yarns, which was examined in a similar manner in results reported
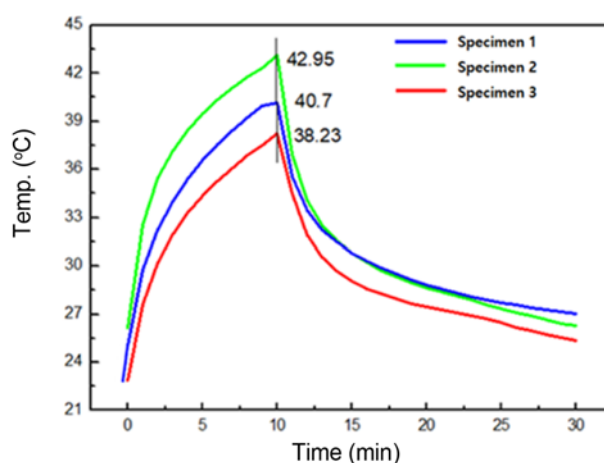

Figure 4. Light heat-emission diagram of fabric specimens according to time.

Table 3. Emissivity and emissive power of yarn specimens

	Specimens (yarn)	Emissive power (W/m^2)	Emissivity (-)
1	Sheath/core PET	$3.58×10^2$	0.881
2	Dispersed PET	$3.65×10^2$	0.894
3	Regular PET	$3.52×10^2$	0.865

previously for ZrC-imbedded PET yarns [7,8]. In addition, the heat-release temperature of the Al_2O_3/graphite-dispersed fabric (specimen 2) was higher than that of the Al_2O_3/graphite sheath/core fabric (specimen 1).

This indicates that the far-infrared absorbing power of the dispersed fabric with Al_2O_3/graphite particles distributed over the whole yarn cross-section is more effective than that of the Al_2O_3/graphite sheath/core fabric with particles imbedded only in the core part of the yarn. This was verified by the far-infrared emission characteristics of the yarn specimens, which was similarly investigated in previous studies [7,8] for ZrC-imbedded PET yarns. Table 3 lists the emissive power and emissivity of the three yarn specimens.

As shown in Table 3, the emissivity and emissive power of the Al_2O_3/graphite-imbedded yarns (specimens 1 and 2) were higher than those of the regular PET yarn (specimen 3), which indicates that the Al_2O_3/graphite-imbedded fabric specimens were more effective for far-infrared emission than the regular PET fabric specimen was. In addition, the effectiveness of the Al_2O_3/graphite-dispersed yarn (specimen 2) was higher than that of the sheath/core yarn (specimen 1), i.e., the higher emissivity and emissive power caused the higher surface temperature of the dispersed fabric than that of the sheath/core fabric. Our measured emissivity values of 0.881 and 0.894 (Table 3) were slightly lower than that previously reported (0.906) for ZrC-imbedded PET yarn [7, 8].

Moisture Absorption and Drying Properties of the Al₂O₃/Graphite Sheath/Core and Dispersed Fabrics

Many measurement methods for the moisture absorption and drying properties have been used to test the perspiration absorption and fast drying properties of woven fabrics. Recently, MMT was designed to measure the liquid moisture transport behaviors in multiple directions [16]. In this study, MMT was used to evaluate the moisture absorption and drying properties of the fabric specimens, as listed in Table 4 for the three fabric specimens. Figure 5 presents the diagrams of the wetting time, absorption rate, MWR, and spreading speed of the three fabric specimens.

As shown in Figure 5(a), the wetting times of the sheath/core and dispersed fabrics (specimens 1 and 2) were shorter than that of the regular PET fabric (specimen 3). This indicates that the moisture absorption of the Al_2O_3/graphite-imbedded PET fabrics is superior to that of the regular PET fabric, which was attributed to the rapid drying of absorbed water in the yarn by the accelerated heat particles generated from the far-infrared radiated by the Al_2O_3 and graphite ceramic particles in the yarn, i.e. accelerated heat particles by far-infrared radiation push out moisture vapor in the yarn and fabric, which makes a rapid drying, and the rapid drying by the heat particles raises the capillary wicking toward the horizontal and vertical directions in the yarn, thereby shortening the wetting time. This was in accordance with the reports by Bahng and Lee [5] of superior sweat-absorbing and fast-drying properties for the Al_2O_3/SiO_2-imbedded

fabric compared to those of the specially designed fast-drying fabrics. In addition, the wetting time of the Al_2O_3/graphite sheath/core fabric (specimen 1) was slightly longer than that of the Al_2O_3/graphite-dispersed fabric (specimen 2), which indicates that the sheath/core fabric has an inferior moisture absorption compared to the dispersed fabric. This was attributed to the lower heat release due to the lower emissivity of the sheath/core fabric than that of the dispersed fabric, as previously explained in Table 3 and Figure 4. On the other hand, as shown in Figure 5(b), the absorption rate of the sheath/core and dispersed fabrics (specimens 1 and 2) was higher than that of the regular PET fabric (specimen 3), which was attributed to the fast drying property of the Al_2O_3/graphite-imbedded yarns, as mentioned previously. In addition, the absorption rate of the sheath/core fabric (specimen 1) was lower than that of the dispersed fabric (specimen 2), i.e., the moisture absorption of the sheath/core fabric was inferior to that of the dispersed fabric, which may be explained in a similar manner to that mentioned previously. Figure 5(c) shows the MWR which affects the drying time of the fabric [16]. The MWR of the sheath/core and dispersed fabrics (specimens 1 and 2) was larger than that of the regular PET fabric (specimen 3), which indicates that the drying properties of the Al_2O_3/graphite-imbedded fabrics are superior to those of the regular PET fabric. This suggests that, because of the high heat release by high emissivity of the Al_2O_3/graphite-imbedded yarns, the test water dropped in the MMT apparatus is absorbed and dried
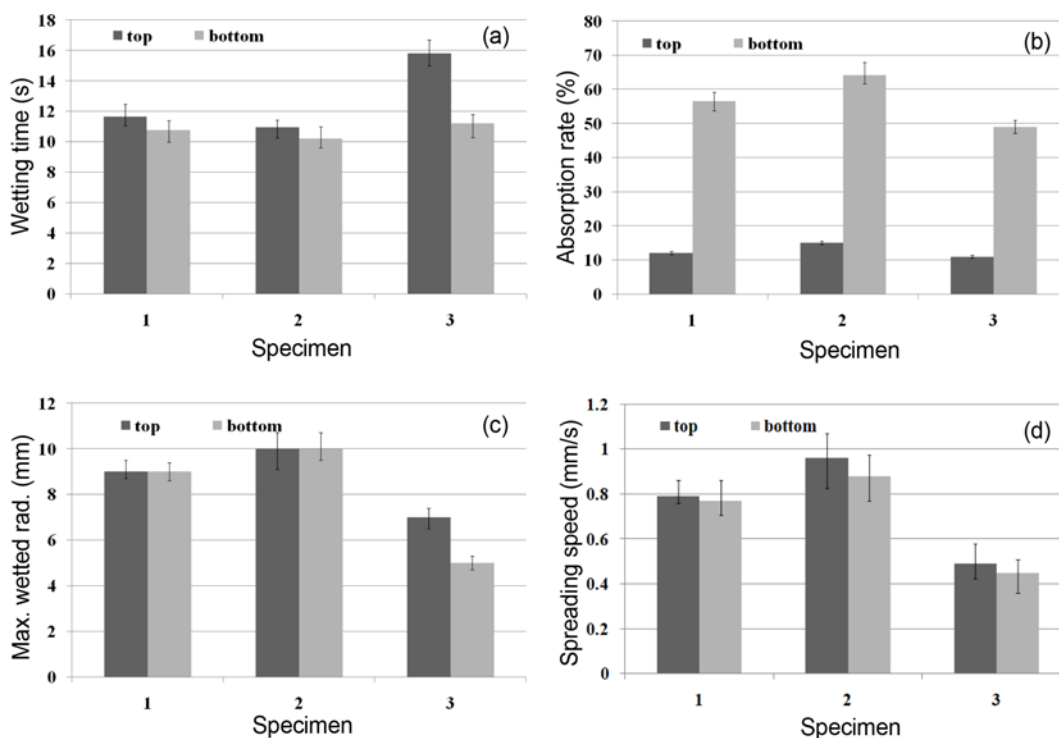

Figure 5. MMT results of the fabric specimens; (a) wetting time, (b) absorption rate, (c) max. wetted rad, and (d) spreading speed.

Table 4. Thermal properties of the fabric specimens

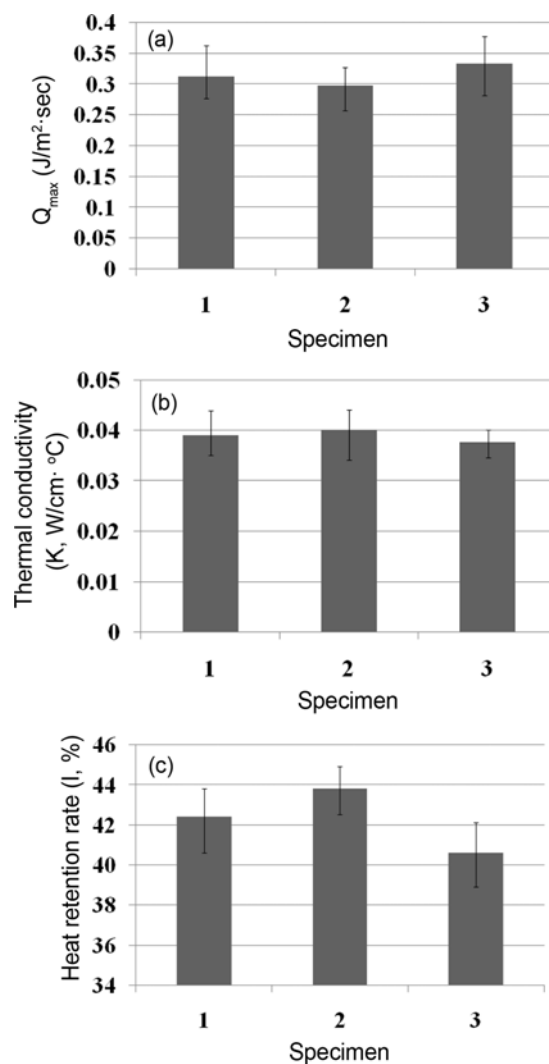|	Specimens	Thermal property					
		Q_{max} (J/m^2·sec)		Thermal conductivity (K, W/cm·^{o}C)		Heat retention rate (I, %)	
		Mean	Dev.	Mean	Dev.	Mean	Dev.
1	Sheath/core PET	0.312	0.085	0.0390	0.009	42.4	3.2
2	Dispersed PET	0.297	0.070	0.0401	0.01	43.8	2.4
3	Regular PET	0.332	0.095	0.0376	0.0055	40.6	3.2

note : dev. = max − min.

rapidly by heat particles radiated from Al_2O_3 and graphite in the yarn, and penetrates rapidly into yarns, which results in a short wetting time and an increase in the absorption rate and MWR. This result indicates that the Al_2O_3/graphite-imbedded fabrics (specimens 1 and 2) have rapid absorbing and fast drying properties, which makes them comfortable to wear [16]. Comparing between specimens1 and 2, the MWR of the sheath/core fabric (specimen 1) was smaller than that of the dispersed fabric (specimen 2), i.e.,it exhibited inferior drying property due to the lower emissivity of the sheath/core fabric than the dispersed fabric did. Figure 5(d) shows the spreading speed (mm/s) of the fabric specimens. The spreading speed of the Al_2O_3/graphite-imbedded fabrics was 1.65-1.95 times faster than that of the regular PET fabric. This result determined by the MMT was in accordance with previous findings [5,7], which were carried out using the MMT methods [5] and wicking experiment (Bireck method) for absorption and drying properties [7]. In addition, the spreading speed of the sheath/core fabric was 17 % slower than that of the dispersed fabric. This result may be explained in a similar manner to that mentioned previously, i.e., the superior moisture absorption and drying properties of the dispersed fabric were attributed to the higher heat release from the surface of the Al_2O_3/graphite-dispersed yarn with Al_2O_3/graphite particles distributed over the whole yarn cross-section than that released from the core part of the sheath/core yarn.

Thermal Properties of the Al_2O_3/Graphite Sheath/Core and Dispersed Fabrics

The manner in which the thermal wear comfort of the fabric is influenced by the heat storage and release properties of the Al_2O_3/graphite sheath/core and dispersed fabrics is also important. The thermal wear comfort properties such as Q_{max}, thermal conductivity (K) and heat retention rate (I) of the fabric specimens were measured using a KES-F7 measuring apparatus. The experimental results are shown in Table 4. An ANOVA analysis (F-test) was performed to verify the statistical significance of the experimental data shown in Table 4. The statistical analysis was carried out between each specimen for mean value of the three thermal properties (Q_{max}, thermal conductivity (K), and heat retention rate (I)) with 95 % confidence limit (5 % of significance

Table 5. ANOVA analysis of the thermal properties

Item	F_0 (V/V$_e$)	p-value	F(2, 27, 0.95)
Q_{max}	44.04	0.029	3.354
K	4.40	0.022	3.354
I	29.27	1.73E-07	3.354

Figure 6. Diagram of thermal properties of the fabric specimens; (a) Q_{max}, (b) thermal conductivity, and (c) heat retention rate.

level). As shown in Table 5, the mean value of the 3 specimens for Q_{max} was statistically significant, as F_0 (V/V$_e$) > F(2, 27, 0.95) and $p<0.05$. Similarly, thermal conductivity and heat retention rate were statistically significant, as F_0 (V/V$_e$) > F(2, 27, 0.95), and $p<0.05$, as shown in Table 5. Figure 6 presents the thermal properties of the fabric specimens.

Q_{max} means the maximum heat flux at the transient state, i.e., the maximum heat amount flowing out from the skin as soon as the fabric contacts to the skin of the human body, which is defined as a measure of the coolness feeling. As shown in Figure 6(a), Q_{max} of the Al$_2$O$_3$/graphite-imbedded fabric specimens was lower than that of the regular PET fabric specimen, which is explained on the basis that the thermal energy accumulated in the Al$_2$O$_3$/graphite-imbedded fabrics by highly emitted far-infrared inhibits the heat flow at the transient state between the human body and the fabrics, resulting in lower Q_{max}. Similar findings were reported by Shim *et al.* [17] and Yeo *et al.* [18], which were carried out using ceramic-coated fabrics. In addition, Q_{max} of the sheath/core fabric specimen was higher that of the dispersed fabric specimen, which was attributed to the lower emissivity of the sheath/core yarn fabric than that of the dispersed yarn fabric (Table 3), resulting in higher Q_{max}. On the other hand, the thermal conductivity (K) of the Al$_2$O$_3$/graphite-imbedded fabrics was higher than that of the regular PET fabric, which was attributed to the higher thermal conductivity of the Al$_2$O$_3$/graphite in the ceramic imbedded yarns than that of the TiO$_2$ imbedded in the regular yarn [19]. This result was consistent with a previous finding [7], which reported that the thermal conductivity of the ZrC-imbedded fabric was higher than that of the regular PET fabric because of the higher thermal conductivity of the ZrC imbedded in the developed yarn than that of TiO$_2$ in the regular yarn. The thermal conductivity of the sheath/core fabric was slightly lower than that of the dispersed fabric, which was attributed to the narrow distribution of the sheath/core yarns, compared to the wide distribution over the whole yarn cross-section of the Al$_2$O$_3$/graphite particles in the dispersed yarns, i.e., the Al$_2$O$_3$/graphite particles imbedded only in the core part of the sheath/core yarn are less effective in thermal conduction than are the dispersed yarns with particles distributed over the whole yarn cross-section, which results in lower thermal conductivity of the sheath/core fabric. As shown in Figure 6(c), the heat retention rate

of the Al$_2$O$_3$/graphite-imbedded fabrics was higher than that of the regular PET fabric, which was attributed to the higher far-infrared radiation emitted from the Al$_2$O$_3$/graphite particles in the yarns (higher emissivity in Table 3), which imparts more heat-generating and storage properties in the Al$_2$O$_3$/graphite-imbedded fabrics, resulting in higher heat retention rate. Similar findings were reported by previous studies [7,17], which reported higher heat retention rates of various ceramic-imbedded fabrics compared to regular PET fabric. The Al$_2$O$_3$/graphite sheath/core fabric exhibited lower heat retention rate than the dispersed fabric did, which may be explained in a similar manner to that previously mentioned, i.e., due to less heat emitted from the core part in the sheath/core yarn than the dispersed yarn with Al$_2$O$_3$/graphite particles distributed over the whole yarn cross-section.

Tactile Hand Feel of the Al$_2$O$_3$/Graphite Sheath/Core Fabrics

This study also examined how the tactile hand of the Al$_2$O$_3$/graphite sheath/core and dispersed fabrics is influenced by the ceramic particles imbedded only in the core of the yarn and distributed over the whole yarn cross-section, respectively. The tactile hand feel of the Al$_2$O$_3$/graphite-imbedded fabrics was estimated from the mechanical properties measured using the FAST system. Table 6 presents the mechanical properties of the three fabric specimens measured by the FAST system. Figure 6 shows the relative mechanical properties of the two types of Al$_2$O$_3$/graphite-imbedded fabric compared to a regular PET fabric. The extensibility (E20 and E100), shear modulus (G), bending rigidity (B) and compressibility (ST) of the two types of Al$_2$O$_3$/graphite-imbedded fabric were plotted as a ratio to those of the regular PET fabric.

As shown in Figure 7, the extensibilities (E20 and E100) of the Al$_2$O$_3$/graphite sheath/core and dispersed fabrics were lower than those of the regular PET fabrics, respectively, which was attributed to the protection afforded by the Al$_2$O$_3$ and graphite nanoparticles imbedded in the yarns from the longitudinal deformation by extension of the fabrics, resulting in lower extensibility. In addition, the extensibility of the sheath/core fabric was higher than that of the dispersed fabric, which indicates that the sheath/core yarns imbedded with the Al$_2$O$_3$/graphite in the core enable the

Table 6. The mechanical properties of the fabric specimens

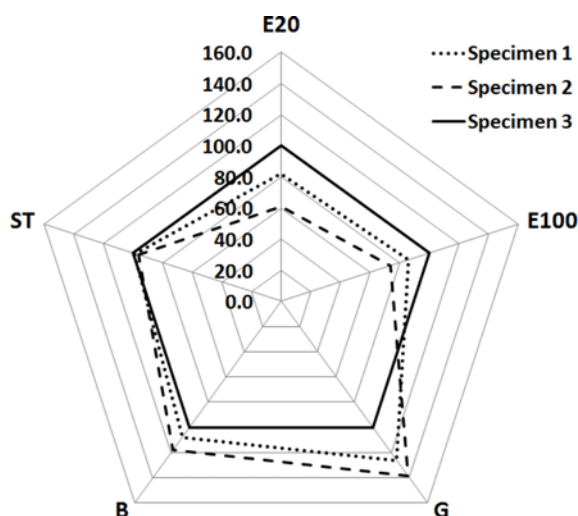|	Specimen no.	Extension				Shear	Bending		Compression
		E20 (%)		E100 (%)		G	B (μN·m)		ST
		Wp	Wf	Wp	Wf	(N/m)	Wp	Wf	(mm)
1	Sheath/core PET	0.1	0.17	0.23	0.63	123.2	71.0	28.0	0.080
2	Dispersed PET	0.1	0.10	0.21	0.53	135.2	78.2	30.2	0.078
3	Regular PET	0.1	0.23	0.27	0.73	97.8	65.7	26.2	0.081

Figure 7. Relative mechanical properties of the ceramic imbedded fabrics compared to the regular PET fabric.

fabric to be more extensible than the dispersed yarn with particles distributed over the whole yarn cross-section. On the other hand, the shear modulus of the Al_2O_3/graphite sheath/core and dispersed fabrics was higher than that of the regular PET fabric. The Al_2O_3/graphite particles imbedded in the yarns prohibit the fabric from the in-plane deformations of the shear and extension of the fabric, which causes high shear modulus and low extensibility. In addition, the shear modulus of the sheath/core fabric was lower than that of the dispersed fabric, which may be explained in a similar manner to the extensibility, indicating that the sheath/core fabric is more extensible in the bias direction than the dispersed fabric is, i.e., it has lower shear modulus. Similarly to the shear modulus, the bending rigidity of the Al_2O_3/graphite sheath/core and dispersed fabrics was higher than that of the regular PET fabric, which reveals the higher stiffness of the Al_2O_3/graphite-imbedded fabrics. In addition, the bending rigidity of the sheath/core fabric was lower than that of the dispersed fabric, indicating that the sheath/core fabric is less rigid and more flexible than the dispersed fabric, which can be explained in a similar manner to that previously mentioned for the extensibility. The compressibility (ST) of the Al_2O_3/graphite sheath/core and dispersed fabrics was slightly lower than that of the regular PET fabric, which indicates that the Al_2O_3/graphite-imbedded fabrics are less compressible than the regular PET fabric due to the Al_2O_3/graphite particles imbedded in the yarns. Regarding the compressibility between the Al_2O_3/graphite sheath/core and the dispersed fabrics, the sheath/core fabric exhibited higher compressibility than the dispersed fabric did, which may be explained in a similar manner to that mentioned in bending. Figure 2 shows that the Al_2O_3/graphite particles (Figures 2a and b) were larger than the TiO_2 particles in the regular PET yarn (Figure 2c), which imparted low extensibility and

compressibility as well as high bending and shear rigidities to the Al_2O_3/graphite-imbedded fabrics. This indicates that the tactile hand feel of the Al_2O_3/graphite-imbedded fabrics is inferior to that of the regular PET fabric, even though they have better wear comfort properties than that of the regular PET fabric due to the higher heat release and storage characteristics by the far-infrared radiation. It has previously been reported [8] that the ZrC particles imbedded in the yarns impart an unpleasant effect on the fabric tactile feel, which was consistent with the current finding. In addition, summarizing the tactile hand feel of the Al_2O_3/graphite sheath/core and dispersed fabrics, the sheath/core fabric appeared to have a soft tactile hand feel compared to the dispersed fabric due to lower extensibilities in the longitudinal and bias directions, and lower bending rigidity with slightly higher compressibility. This result suggests that the Al_2O_3/graphite sheath/core fabric has strong potential for commercial applications such as soft tactile hand feel with no color problem in dyeing, despite its slight inferior wear comfort properties such as moisture absorption and heat retention rate (MMT and I values), as well as lower heat storage and release properties compared to those of the dispersed fabric.

Conclusion

The wear comfort properties of ceramic-imbedded fabrics were examined with the heat storage/release characteristics according to ceramic-imbedded PET yarn structure in terms of the maximum surface temperature, moisture absorption and drying, and heat retention rate measured using a light heat emission apparatus, an MMT, and a thermal property measuring system (KES-F7). These results were verified by the far-infrared emissivity and elemental analysis of the yarn specimens. In addition, the tactile hand feel of the ceramic-imbedded fabrics according to the yarn characteristics was estimated from the fabric mechanical properties measured by the FAST system. The maximum surface temperature of the Al_2O_3/graphite sheath/core yarn fabric was lower than that of the Al_2O_3/graphite-dispersed yarn fabric. The moisture absorption and drying properties measured by the MMT of the Al_2O_3/graphite sheath/core yarn fabric were inferior to those of the dispersed yarn fabric. Concerning the thermal properties, the heat retention rate and thermal conductivity of the sheath/core yarn fabric were lower and the Q_{max} value was higher than those of the dispersed yarn fabric. These findings related to the wear comfort properties revealed that the sheath/core yarn fabric exhibited inferior wear comfort properties compared to those of the dispersed yarn fabric, which was attributed to the lower heat release from the core part of the sheath/core yarn than that released from the dispersed yarn with Al_2O_3/graphite particles distributed over the whole yarn cross-section. This was verified by the lower emissivity and emissive power of the

sheath/core yarn than those of the dispersed yarn. The sheath/core yarn fabric appeared to have a softer tactile hand feel compared to the dispersed yarn fabric. In addition, both sheath/core and dispersed yarn fabrics exhibited better wear comfort properties than the regular PET fabric did, but imparted an uncomfortable tactile hand feel compared to the regular PET fabric. Finally, this study revealed the superior moisture absorption/drying properties and thermal characteristics of the Al_2O_3/graphite dispersed yarn fabric (i.e. better wear comfort) compared to the sheath/core yarn fabric. It suggests that higher heat retention rate and thermal conductivity with lower Q_{max} of the Al_2O_3/graphite dispersed yarn fabric are appropriate for winter clothes. However, the dispersed yarn fabric exhibited an uncomfortable hand feel compared to the sheath/core yarn fabric, which needs in depth consideration in further study.

References

1. W. Xu, T. Shyr, and M. Yao, *Text. Res. J.*, **77**, 513 (2007).
2. D. M. Anderson, J. R. Fessler, M. A. Pooley, S. Seidel, M. R. Hamblin, H. W. Beckham, and J. F. Brennan III, *Bio Medical Opt. Express*, **8**, 1698 (2017).
3. M. A. Pooley, D. M. Anderson, H. W. Beckham, and J. F. Brennan III, *Opt. Express*, **24**, 10556 (2016).
4. T. Furata, Y. Shimizu, and Y. Kondo, *Text. Res. J.*, **66**, 123 (1996).
5. G. W. Bahng and J. D. Lee, *Text. Res. J.*, **84**, 1220 (2014).
6. C. F. J. Kuo, C. C. Fan, T. L. Su, S. H. Chen, and W. L. Lan, *Text. Res. J.*, **86**, 1677 (2016).
7. H. A. Kim and S. J. Kim, *Autex. Res. J.*, **17**, 142 (2017).
8. H. A. Kim and S. J. Kim, *Autex. Res. J.*, **19**, 165 (2019).
9. C. A. Lin, T. C. An, and Y. H. Hsu, *Pol. Plastics Tech. Eng.*, **46**, 1073 (2007).
10. J. H. Lin, C. L. Huang, Z. I. Lin, and C. W. Lou, *J. Com. Mat.*, **50**, 2099 (2016).
11. C. M. Lin and C. W. Chang, *Text. Res. J.*, **78**, 555 (2008).
12. J. H. Lin, J. C. Jhang, T. A. Lin, S. Y. Huang, Y. S. Chen, and C. W. Lou, *Fiber. Polym.*, **18**, 597 (2017).
13. Entergris, Properties and Characteristics of Graphite, https://www.entegris.com/content/dam/web/resources/brochures/brochure-properties-and-characteristics-of-graphite-7329.pdf (Accessed May 20, 2020).
14. H. A. Kim and S. J. Kim, *Text. Res. J.*, **89**, 1394 (2019).
15. Commonwealth Scientific and Industrial Research Organization (Australia) Division of Wool Technology, "Wool Technology", p.29, Geelong, Vic. : CSIRO, Australia, 1989.
16. G. Supuren, N. Oglakcioglu, N. Ozdil, and A. Marmarali, *Text. Res. J.*, **81**, 1320 (2011).
17. M. H. Shim, C. H. Park, and H. S. Shim, *Text. Res. J.*, **79**, 1557 (2009).
18. S. Y. Yeo, D. H. Lee, and E. A. Kim, *J. Kor. Soc. Clo. Text.*, **22**, 515 (1998).
19. O. K. Kwon, Heat Delivery Mechanism of Textile Products and Development Trend of Keeping Warmth Functionalized Product, http://www.textopia.or.kr/new/index.do (Accessed October 20, 2020).